Electrochemical behavior of LiV_3O_8 positive electrode in hybrid Li,Na–ion batteries

S. Maletti[1,2], A. Sarapulova[1], A. A. Tsirlin[3], S. Oswald[2], F. Fauth[4], L. Giebeler[2], N. N. Bramnik[1], H. Ehrenberg[1], D. Mikhailova[1,2]*

1-*Karlsruhe Institute of Technology (KIT), Institute for Applied Materials (IAM), Hermann-von-Helmholtz-Platz 1, D-76344 Eggenstein-Leopoldshafen, Germany*

2-*Leibniz Institute for Solid State and Materials Science (IFW) Dresden e.V., Institute for Complex Materials, Helmholtzstr. 20, D-01069 Dresden, Germany*

3-*University of Augsburg, Experimental Physics VI, Center for Electronic Correlations and Magnetism, Universitaetsstr. 1, D-86159 Augsburg, Germany*

4-*CELLS-ALBA Synchrotron, Carrer de la Llum 2-26, E-08290 Cerdanyola del Vallès, Barcelona, Spain*

Corresponding E-mail: daria.mikhailova@kit.edu

Keywords: Li,Na-hybrid cells, co-intercalation of Li and Na cations, Li and Na diffusion coefficients in LiV_3O_8

Abstract

Vanadium(V)-containing oxides show superior intercalation properties for alkaline ions, although the performance of the material strongly depends on its surface morphology. In this work, intercalation activity of LiV_3O_8, prepared by a conventional solid state synthesis, is demonstrated for the first time in non-aqueous Li,Na-ion hybrid batteries with Na as negative electrode, and different Na/Li ratios in the electrolyte. In the pure Na-ion cell, one Na per formula unit of LiV_3O_8 can be reversibly inserted at room temperature via a two-step process, while further intercalation leads to gradual amorphisation of the material, with a specific capacity of 190 $mAhg^{-1}$ after 10 cycles in the potential window of 0.8-3.4 V. Hybrid Li,Na-ion batteries feature simultaneous intercalation of Li^+ and Na^+ cations into LiV_3O_8, resulting in the formation of a second phase. Depending on the electrolyte composition, this second phase bears structural similarities either to $Li_{0.7}Na_{0.7}V_3O_8$ in Na-rich electrolytes, or to $Li_4V_3O_8$ in Li-rich electrolytes. The chemical diffusion coefficients of Na^+ and Li^+ in crystalline LiV_3O_8 are very close, hence explaining the co-intercalation of these cations. As DFT calculations show, once formed, the

$Li_{0.7}Na_{0.7}V_3O_8$-type structure favors intercalation of Na^+, whereas the LiV_3O_8-type prefers to accommodate Li^+ cations.

Introduction

Nowadays sodium-ion batteries are recognized as promising candidates for stationary energy storage applications due to the low cost and abundance of sodium [1-3]. Despite the larger ionic radius of Na^+ in comparison to Li^+ (1.02 Å *vs*. 0.76 Å for the octahedral oxygen surrounding [4]), fast kinetics with Na^+ as charge carrier could nevertheless be expected, since *i*) weaker Lewis acidity of the Na^+ cations reduces their solvation energy, hence facilitating their transfer at the electrolyte/electrode phase boundary [5], and *ii*) larger polarizability of Na^+ can reduce the activation barrier for diffusion in the bulk [6].

Since the operation principle of sodium-ion cells is very similar to lithium-ion batteries, many of the lithium insertion compounds may be considered as sodium insertion hosts and thus as electrode materials for sodium-ion batteries. Polyanionic Li- and Na-insertion positive electrodes with three-dimensional structures or two-dimensional layered structures containing vanadium(V), are of special interest owing to the variable oxidation state of vanadium, which may facilitate multi-electron redox processes and high theoretical capacities. However, the preparation of Na-containing materials, which are isostructural to the corresponding Li-compounds, requires often a complicated synthesis procedure different from the one for the Li-analogue as in the case of olivine-like $NaFePO_4$ [7]. Moreover, the larger size of Na^+ puts additional restrictions on the host structures that should sustain larger lattice expansion. Many of the materials undergo amorphisation or show lower capacity values upon repeated cycling with Na^+ intercalation.

In order to overcome this drawback, an innovative concept of hybrid non-aqueous Li^+/Na^+ rechargeable batteries can be proposed following the widely studied Li,Mg-hybrid cells [8-10]. These cells feature a Mg anode and an electrolyte composed of Mg- and Li-salts, thus using advantages of both ingredients. While Mg is abundant and evades dendrite formation, Li^+ supports fast diffusion in the bulk and allows a large choice of suitable high capacity electrode materials. In the ideal case, the exchange of the smaller Li^+ ions should occur between the electrolyte and the positive electrode (“cathode”), while the divalent Mg^{2+} ions are exchanged between the electrolyte and the negative electrode (“anode”). During cell charge and discharge, the total concentration of Li^+ and Mg^{2+} ions in the electrolyte provides

charge neutrality, but the Li^+/Mg^{2+} ratio is changed [9]. The capacity, operating voltage in terms of cell polarisation, and the stability of such batteries depend on the electrolytes [9]. However, simultaneous intercalation of both metal ions into one electrode can also occur, provided that the insertion potentials and intercalation kinetics are similar for both ions [11].

Up to now, most studies were focused on the mixed-ion Li,Mg- [8-10], Na,Mg- [12, 13], and aqueous Li,Na- [14] hybrid batteries. To the best of our knowledge, the only implementation of the mixed Li,Na-battery reported so far involves a Li_2RuO_3 positive electrode, a Na negative electrode, and a purely Na-salt electrolyte [15]. However, the total amount of Li in the electrolyte did not exceed 4% after complete cell charge, and common principles of Li,Na-hybrid cells could not be studied in this system.

Layered lithium vanadium(V) oxide, LiV_3O_8, is a promising positive electrode material for such hybrid Li,Na-cells. This compound has been studied since the 1980s as positive electrode in non-aqueous Li-ion batteries [16-18] and as negative electrode in aqueous rechargeable Li-ion batteries [19]. Although the use of vanadium implies similar concerns in terms of environmental compatibility and sustainability as commercially applied Co-, Ni- and Mn-containing materials, LiV_3O_8 is considered superior to common positive electrode materials due to its outstanding electrochemical performance. During Li-insertion, more than 3 Li^+ ions per formula unit can be reversibly inserted into the structure between vanadium-oxygen layers, resulting in the valence state of vanadium below 4+. As the pristine compound exists in charged state, a lithium-containing negative electrode is needed. The crystal structure does not undergo significant transformations upon Li-insertion [20], see Fig. 1a. The most important changes include some shifts of metal and oxygen atoms resulting in the transformation of VO_5 pyramids into distorted VO_6 octahedra. The Na-insertion into this compound was not studied so far, although a mixed Li,Na vanadium oxide with a related structure is known, see Fig. 1b [21]. In a Li,Na-hybrid cell, one could expect mostly Li intercalation because of its smaller ionic radius in comparison to Na^+ as well as a larger thermodynamic stability of the lithiated phase compared to the sodiated one, because of the larger repulsion between the Na and Li ions in the $NaLiV_3O_8$ structure than in $Li_2V_3O_8$.

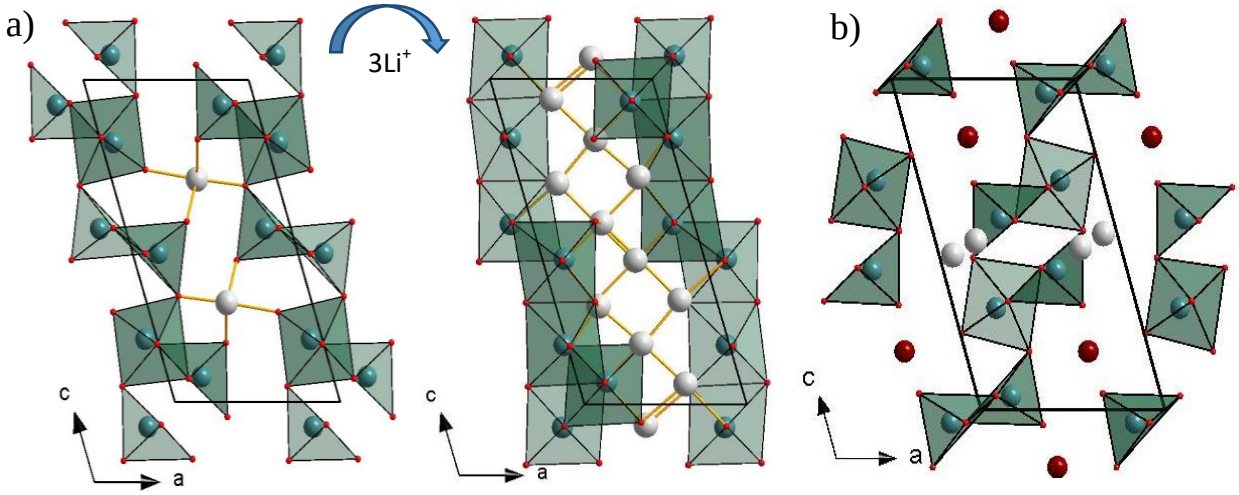

Figure 1. a) Monoclinic structures of initial LiV_3O_8 (left) and lithiated $Li_4V_3O_8$ (right) along the *b*-axis, according to [20]. Upon lithiation, the lattice parameters *a* and *b* noticeably increase, while the parameter *c* slightly decreases. b) Monoclinic structures of $Li_{0.7}Na_{0.7}V_3O_8$ [21]. The grey and brown spheres are lithium and sodium cations, respectively; vanadium cations are inside the green polyhedra.

In the present work, we study LiV_3O_8 as a host material in hybrid Li,Na-cells with a Na-anode and different Li and Na cation compositions of the electrolyte. We show that 1 Na per LiV_3O_8 formula unit can be reversibly intercalated into pure Na-cells *via* a two-phase process without any structural decomposition. In Li,Na-hybrid cells, electrochemical behavior of LiV_3O_8 was studied in dependence on the Li/Na cation ratio in the electrolyte, also from the structural point of view with *in situ* experiments. Simultaneous intercalation of the Li^+ and Na^+ cations into LiV_3O_8 is established in hybrid cells with equal availability of both kind of cations in the electrolyte because of kinetic and thermodynamic considerations. At the same time, Li-deposition on metallic Na was observed upon the first cell charge, thus leading to an “inverse” hybrid cell, in which Li^+ ions are mostly exchanged between the negative electrode and electrolyte, while Na^+ ions shuffle between the electrolyte and the positive electrode. Possible reasons behind this behavior are discussed.

Experimental

Synthesis and characterization

LiV_3O_8 samples were prepared by solid-state reaction from stoichiometric amounts of Li_2CO_3 (Fluka, 98,0 %) and NH_4VO_3 (Merck, 99,0 %) placed in Al_2O_3 crucibles at 500 °C for 40 h and cooled down to room temperature. Since particle size of the active material affects its electrochemical performance, one LiV_3O_8 sample was ball-milled (Fritsch Pulverisette 7) in an Ar-filled glove-box at room temperature for 2.5 h at 300 rpm using a grinding bowl and grinding balls from tungsten carbide, with 10 wt. % Super P carbon (TIMCAL) to reduce the particle size and to coat the particles inherently with carbon for improving electronic conductivity of the material.

Phase analysis and determination of cell parameters of LiV_3O_8 at room temperature were carried out using powder X-ray diffraction with a STOE STADI P diffractometer (Cu-$K_{\alpha1}$ radiation, λ = 1.54059 Å) in transmission mode. Diffraction experiments for phase analysis of sodium-containing materials after electrochemical treatments were performed without any contact of the sample with air by sealing the sample between two polyimide sheets.

Electrochemical investigations

Electrochemical studies on LiV_3O_8 electrodes were performed using a VMP3 (Biologic, France) multichannel potentiostatic−galvanostatic system in standard two-electrode Swagelok-type cells with metallic Na as anode. For the positive electrode, a mixture of LiV_3O_8, super P carbon, and polyvinylidene difluoride (PVDF, Solef 21216) as polymer binder in an 80:10:10 weight ratio was pressed onto steel meshes with 10 mm in diameter and dried under vacuum at 80 °C overnight. A home-made 1 M solution of $NaClO_4$ (ACS, 98-102%) in propylene carbonate PC (Sigma-Aldrich, anhydrous, 99.7%) was used as the electrolyte. The sodium disks serving as anode were home-made by rolling Na-pieces (Alfa Aesar, 99.95%) into thin plates. The cells were assembled in an argon-filled glovebox with H_2O and O_2 contents of less than 1 ppm.

In hybrid Na,Li-cells of Swagelok-type, metallic Na was used as negative electrode, LiV_3O_8 as positive electrode, and a mixed home-made solution of 1M $LiClO_4$ (Sigma-Aldrich, 99.99%) and 1M $NaClO_4$ (1:1) in PC as electrolyte, yielding the total concentration of Li^+ and Na^+ ions of 1M. The $LiClO_4$ and $NaClO_4$ salts were dried at 80 °C under vacuum overnight prior to use.

Chemical diffusion coefficients of Na and Li in crystalline LiV_3O_8 were determined using galvanostatic intermitted titration technique (GITT) in a Swagelok-type three-electrode cell with a Na or Li negative electrode, LiV_3O_8 positive electrode, and a

metallic Na (Li) disk as a reference electrode, following the procedure extensively discussed in the literature [22, 23].

XPS studies

X-ray photoelectron spectroscopy (XPS) was performed on pristine LiV_3O_8 and the products with different sodium contents after electrochemical Na^+ insertion. The PHI 5600 CI system with an Al Kα 350 W monochromatized X-ray source and a hemispherical analyzer at a pass energy of 29 eV were used. Cells with the same electrode mixture consisting of LiV_3O_8, carbon black, and PVDF with a mass of ~20 mg were discharged to 1.45 V and 1.00 V, corresponding to the nominal compositions "$NaLiV_3O_8$" and "$Na_2LiV_3O_8$", and immediately disassembled in the glovebox. In order to remove electrolyte from the surface, the powders were washed twice with DMC. After drying, the samples were transferred from the glovebox into the XPS system in an Ar-filled transfer chamber without any contact to air. During XPS measurements, when necessary, surface charging was minimized by means of a low-energy electron flood gun. The system base pressure was below 10^{-9} mbar. The binding energy scale was calibrated from minor carbon contaminations using the C 1s peak maximum at 284.8 eV.

***In situ* X-ray synchrotron diffraction**

In situ X-ray synchrotron diffraction measurements on LiV_3O_8 in Na, Li- and hybrid Li,Na-cells were performed at the beamline BL04-MSPD [24] at ALBA (Barcelona, Spain) and at the beamline P02.1 at PETRA III/DESY (Hamburg, Germany) in transmission mode. The experimental setup containing a coin cell holder connected to a VMP multichannel potentiostat is described elsewhere [25]. Data were collected in steps of 0.005° at wavelengths of 0.41289(1) Å (ALBA) and 0.20711(1) Å (PETRA III), which were refined from the reflection positions of NIST silicon and LaB_6 reference materials.

In order to characterize pristine LiV_3O_8, a pattern was recorded before starting the electrochemical process. The cell was then successively discharged and charged in galvanostatic mode at a constant current corresponding to the insertion or extraction of 1 Na per formula unit during 10 h (C/10 rate). All diffraction patterns were analysed by Fullprof implemented into the software package WinPLOTR [26]. The Al-foil current collector on the positive electrode side served as an internal standard during the measurements, and the refined lattice parameter of Al provided an independent control of the reliability of the obtained model parameters.

Density-functional calculations

The stability of the LiV_3O_8 structure upon Li and Na intercalation was assessed by density-functional band-structure calculations performed in the VASP code [27, 28] using the Perdew-Burke-Ernzerhof (PBE) flavor of the exchange correlation potential [29]. The DFT+U technique with U_d = 3 eV and J_d = 1 eV was used to account for electronic correlations in the V 3*d* shell, and ferromagnetic order in the intercalated compounds was assumed. Both atomic positions and lattice parameters were fully relaxed in all calculations.

Results and discussion

1. Material characterization

According to laboratory XRD analysis (Fig. S1, Supporting Information), LiV_3O_8 samples prepared *via* solid-state synthesis were single-phase crystallizing in the monoclinic $P2_1/m$ space group with lattice parameters a = 6.6319(1) Å, b = 3.58651(4) Å, c = 11.9714(1) Å, β = 107.8127(8)° in good agreement with the literature data [20]. The cation ratio Li:V = 1:3 in the material was confirmed by ICP-OES analysis after dissolving the sample in HNO_3 solution. In order to reduce the particle size, the material was ball-milled in an Ar-filled glove-box at room temperature with a total milling time of 2.5 h. SEM images of the material before and after milling revealed a change in particle morphology from long plates of about 2 µm to spherical particles with the 200-400 nm diameter, which form large agglomerates of several µm (Fig. S2). XRD pattern of the milled material showed no Bragg reflections (Fig. S3), thus indicating its loss of any long-range order upon milling.

2. Electrochemical behavior and structural evolution of LiV_3O_8 in pure Na-ion cells

Prior to investigating LiV_3O_8 in Li,Na-hybrid cells, we collected versatile information about the behavior of this material in pure Na-ion batteries. We found that crystalline and amorphous LiV_3O_8 showed very different electrochemical behavior as positive electrodes in Na-cells. The crystalline material additionally showed different characteristics depending on the cut-off cell voltage. For comparison, amorphous LiV_3O_8 was also tested in Li-cells (Fig. S4).

First, crystalline LiV_3O_8 was galvanostatically cycled between 0.8 and 3.4 V *vs*. Na^+/Na, as shown in Fig. 2a (right). Irreversible effects were observed: two plateaus

at 2.4 and 1.5 V manifested themselves during the first cell discharge, largely deteriorated during the second discharge, and vanished in further cycles. Therefore, irreversible changes in the active material occur. In fact, XRD of LiV_3O_8 after several cycles between 0.8 and 3.4 V in the Na-cell revealed diffraction patterns typical for materials with a weak crystalline ordering, see Figure S5. In contrast, the discharge-charge curves of LiV_3O_8 cycled between 1.6 and 3.4 V *vs*. Na^+/Na, corresponding to the insertion and removal of 1Na per LiV_3O_8, replicate each other, and XRD patterns after cycling show a well-crystalline material (Figure S5). The resulting capacities for different voltage windows are presented in Fig. 2a (left). The first discharge capacity of 230 $mAhg^{-1}$ typically decreases to 160 $mAhg^{-1}$ in the 20^{th} cycle for Na-cells cycled between 0.8 and 3.4 V *vs*. Na^+/Na, while it shows a very stable behavior with 60 mAh/g upon cycling between 1.6 and 3.4 V. Therefore, LiV_3O_8 reversibly intercalates not only Li^+ cations, but Na^+ cations as well.

The first intercalation plateau in the Na cell at about 2.4 V *vs*. Na^+/Na is about 0.3 V lower than in the case of Li insertion in the Li cell (results not shown here). This behavior indicates that the V^{5+}/V^{4+} redox potentials of both systems are similar, because the 0.3 V difference is directly related to the difference between the Li^+/Li and Na^+/Na redox couples [30].

The cycling of the ball-milled LiV_3O_8 material in Na-cells with different cut-off voltages revealed sloping charge-discharge curves without any noticeable plateaus, as for materials with pronounced (pseudo)capacitive properties. The resulting capacities for both voltage windows, 1.6-3.4 V and 0.2-3.4 V *vs*. Na^+/Na, are comparable starting from the second discharge-charge cycle, as seen in Fig. 2b. However, the cells cycled down to 0.2 V *vs*. Na^+/Na, showed a much faster capacity loss, while cells operated down to 1.6 V indicate stable behavior for the first 10-12 cycles with about 80 $mAhg^{-1}$, followed by a deterioration of the electrochemical capacity.

EDX analysis of LiV_3O_8 electrode materials after one, five and twenty discharge-charge cycles between 1.6 V and 3.4 V in the Na-cells revealed a very homogeneous distribution of Na in particles with nearly the same amount of Na (10 wt.%), as seen in Fig. S6. The presence of the residual Na^+ cations in the material after cell charge may indicate an enhanced thermodynamic stability of the partially sodiated $Na_{0.2}LiV_3O_8$ phase.

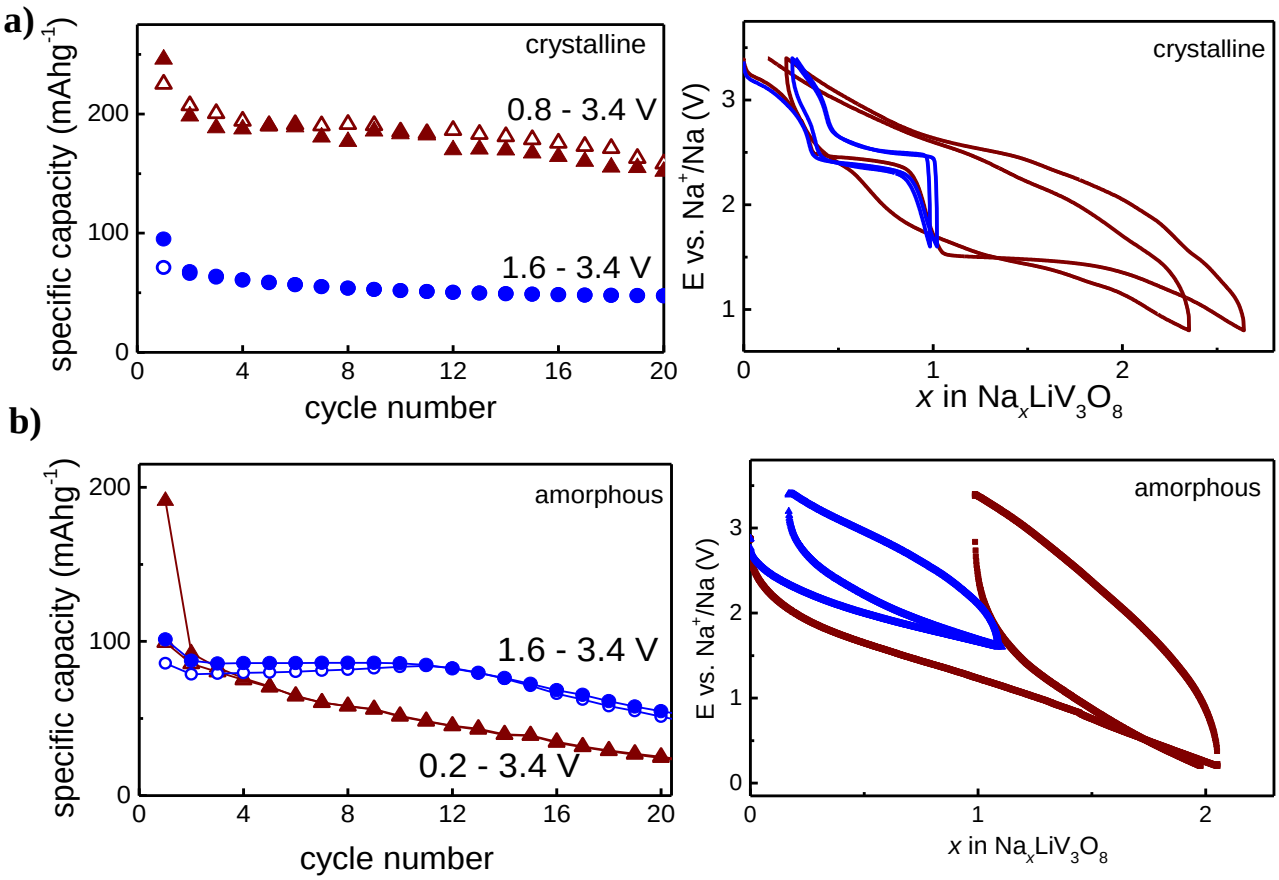

Figure 2. Galvanostatic cycling and charge-discharge capacity (empty and filled symbols, respectively) depending on the cycle number for a) crystalline LiV_3O_8, and b) amorphous LiV_3O_8 positive electrode in Na-cells. The charge/discharge rate corresponds to 1 inserted cation per formula unit during 10 h (C/10).

Kinetics studies of Na^+ diffusion in LiV_3O_8 in the temperature range 10 - 50 °C using GITT technique (see Fig. S7 for a single galvanostatic intermittent titration) revealed chemical diffusion coefficients $\tilde{D}_{Na}$ varying by two orders of magnitude depending on cell voltage for each temperature, see Fig. 3a. For all temperatures, the lowest values for $\tilde{D}_{Na}$ are around 2.4 V that correlates with the plateau in the voltage dependence of the composition (Fig. 3b). As the plateau corresponds to a biphasic reaction, the obtained values do not represent strictly defined diffusion coefficients but values that can be considered an effective measure of the overall kinetics in that region. It was not possible to measure $\tilde{D}_{Na}$ using GITT below 2.0 V, because cell voltage after a current pulse does not reach a steady-state value. Since voltage dependences between 10 °C and 50 °C are similar, the electrochemical processes in this temperature range are also similar.

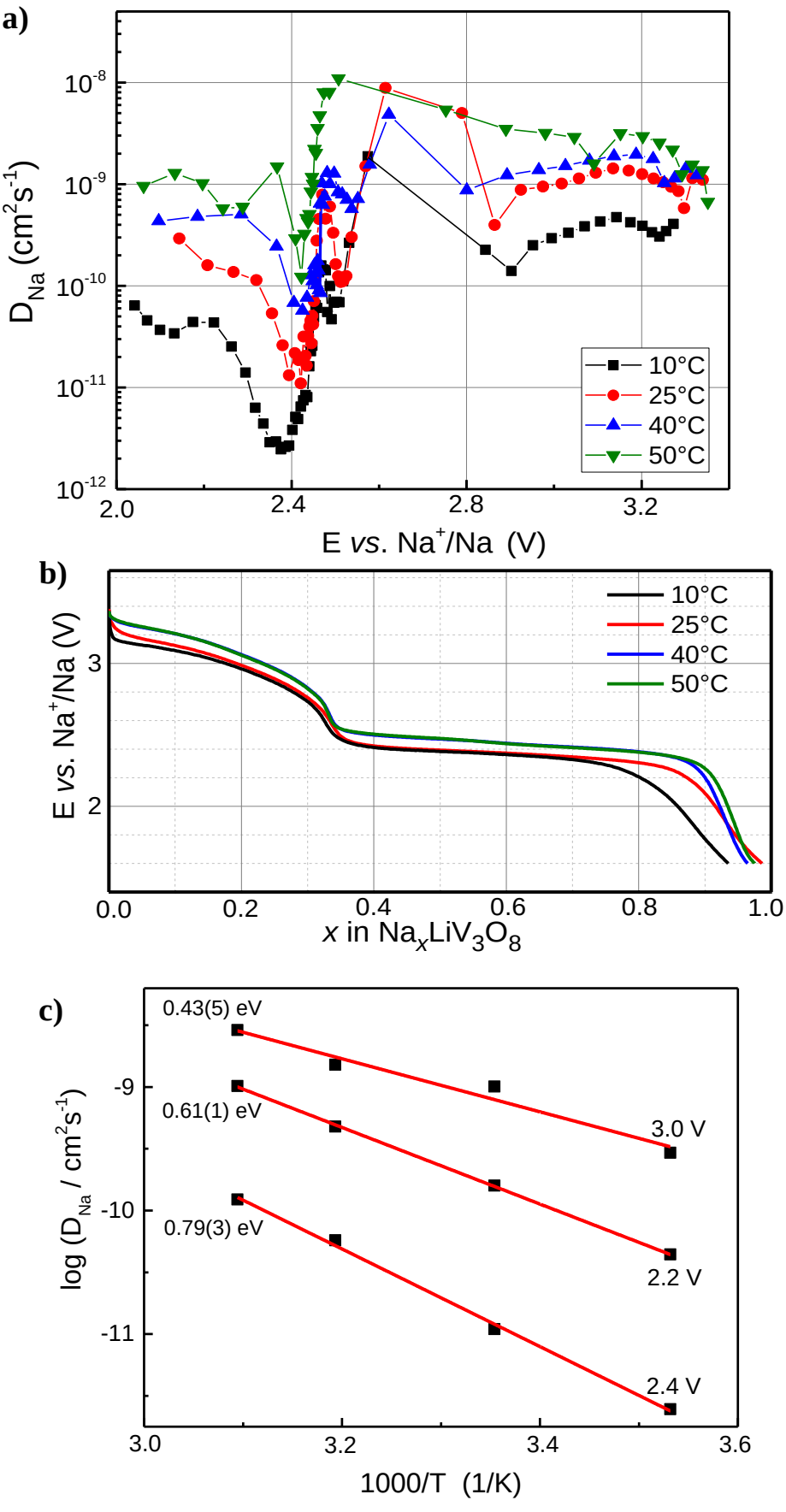
a)
10^{-8}
10^{-9}
10^{-10}
10^{-11}
10^{-12}
D_{Na} (cm^2s^{-1})
2.0
2.4
2.8
3.2
E *vs*. Na^+/Na (V)
10°C
25°C
40°C
50°C
b)
E *vs*. Na^+/Na (V)
3
2
0.0
0.2
0.4
0.6
0.8
1.0
x in $Na_xLiV_3O_8$
10°C
25°C
40°C
50°C
c)
0.43(5) eV
0.61(1) eV
0.79(3) eV
3.0 V
2.2 V
2.4 V
log (D_{Na} / cm^2s^{-1})
-9
-10
-11
3.0
3.2
3.4
3.6
1000/T (1/K)

Figure 3. a) Na^+ diffusion coefficients in LiV_3O_8 as a function of cell voltage during cell discharge at temperatures between 10 °C and 50 °C from GITT. b) Corresponding composition dependences of cell voltage between 10 °C and 50 °C. c) Arrhenius plots for the diffusion coefficients determined for individual electrochemical processes at 2.2, 2.4 and 3.0 V *vs*. Na^+/Na.

From the temperature dependence of the chemical diffusion coefficient $D = D(T)$ the activation energy E_a for the ionic transport can be estimated applying the Arrhenius equation, $D = D_0 \exp(-E_a/RT)$. Activation energies of 0.43 eV, 0.79 eV, and 0.61 eV were calculated for three cell voltages, 3.0 V, ~2.4 V and 2.2 V *vs*. Na^+/Na, respectively, corresponding to different diffusion coefficient values (Fig. 3c). Obviously, the diffusion at 2.4 V is mostly impeded, followed by the process at 2.2 V and 3.0 V.

The XPS characterization of pristine LiV_3O_8 and Na-inserted $NaLiV_3O_8$ and $Na_2LiV_3O_8$ samples (Fig. 4) revealed quite different V2p and O1s spectra showing the reduction in the oxidation state of vanadium and a partial structural decomposition. The O1s spectrum of pristine LiV_3O_8 shows a well-defined main peak at 529.6 eV (green color), which is characteristic for O^{2-} ions in a structural network of oxides [31], and a minor component at 532.0 eV (grey color), which can be attributed to any structural defects in the subsurface-like cation/oxygen deficiency [31]. After insertion of 1 Na per formula unit at 1.45 V vs. Na^+/Na, the lattice O^{2-} peak shifted to higher binding energies reflecting a structural rearrangement upon the reduction of vanadium. In addition, a new peak 533.5 eV appears in the spectrum of $NaLiV_3O_8$ (yellow color), which can be attributed to oxygen of carbonate groups [32], and to Cl-O species [33].

Upon further incorporation of Na into the material, the O1s spectrum drastically changed. It became much broader, the feature at about 530 eV corresponding to the lattice O^{2-} (green color) lost intensity, whereas the carbonate-attributed peak at about 533.5 eV increased significantly, indicating the presence of the sub-surface oxygen mostly in the form of carbonates. This observation is well in line with the decay of $Na_{1+x}LiV_3O_8$ below 1.5 V and the onset of the amorphisation process. Based on the fact that the Na1s peak maxima in $NaLiV_3O_8$ and $Na_2LiV_3O_8$ are offset by 0.35 eV (Fig. 4), and the peak of $Na_2LiV_3O_8$ is actually composed by two peaks, two different states of Na in these materials can be proposed.

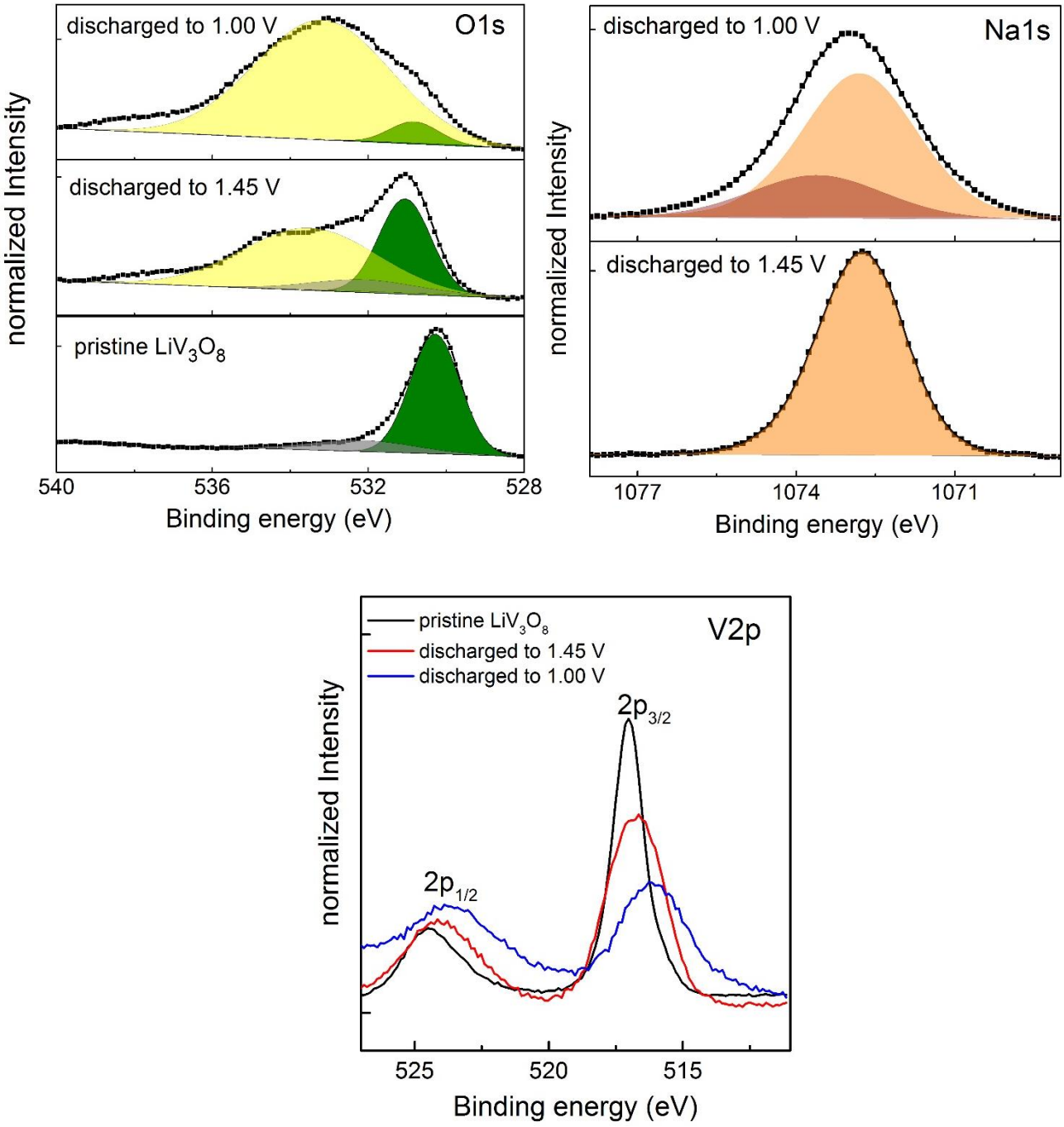

Figure 4. O1s, Na1s and V2p photoelectron spectra of pristine LiV_3O_8, $NaLiV_3O_8$ after discharge to 1.45 V, and $Na_2LiV_3O_8$ after discharge to 1.00 V *vs*. Na^+/Na. The O1s spectrum of pristine LiV_3O_8 comprises one main peak at 529.6 eV (green color) that corresponds to the lattice O^{2-} peak, and a minor component at 532.0 eV (grey color), which can be attributed to structural defects in the subsurface like cation/oxygen deficiency. The incorporation of Na-cations leads to a shift of the main O1s peak

toward higher BE, consistent with structural changes, and to the appearance of an additional peak at 533.5 eV. Upon sodiation, the single $V2p_{3/2}$ peak of pristine LiV_3O_8 becomes broader and shifts toward lower BE, reflecting the reduction of vanadium cations. The Na1s spectra of $NaLiV_3O_8$ and $Na_2LiV_3O_8$ point one and two different states of Na, respectively.

The $V2p_{3/2}$ peak in the V2p spectra shifts towards lower energies upon Na intercalation, which is well in line with the anticipated reduction of vanadium. The broadening of $V2p_{3/2}$ peaks in Na-containing samples may reflect several electronic states of vanadium in the material. Therefore, XPS data unambiguously demonstrate considerable changes in the electronic structure that occur during the intercalation. These changes become even more significant when $NaLiV_3O_8$ is transformed into $Na_2LiV_3O_8$. This behavior coincides with the decomposition/amorphisation of $Na_2LiV_3O_8$.

Structural changes upon sodiation and subsequent desodiation of LiV_3O_8 were investigated using *in situ* synchrotron powder diffraction. A Na-cell was discharged to 1.6 V *vs*. Na^+/Na and charged to 3.4 V. The evolution of the diffraction patterns as a function of cell voltage is presented in Fig. 5a. Clearly, the appearance of new reflections at high *d*-values, as for example at $d \approx 7$ Å, can be observed. These reflections are retained and become even more pronounced after subsequent Na extraction from the structure upon cell charge. Evolution of other reflections upon cation insertion and extraction (for example, at $d \approx 3.45$ and $d \approx 2.60$ Å) indicates a conventional cell expansion/shrinkage.

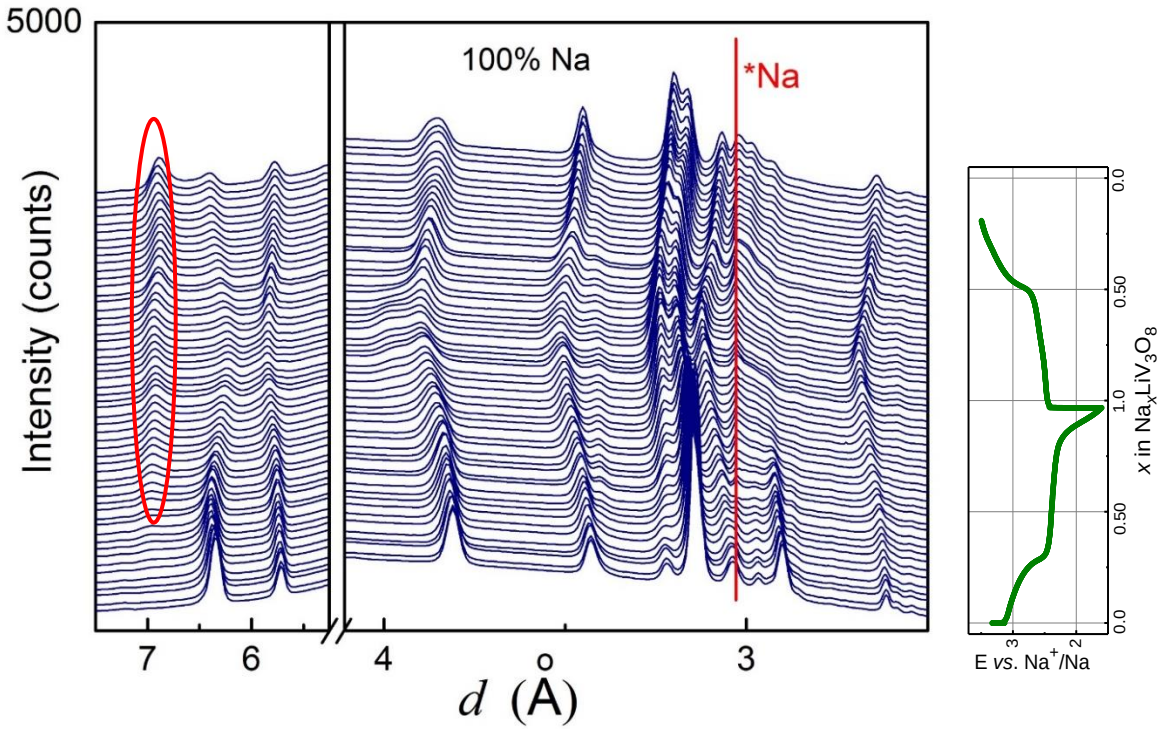

Figure 5a. *In situ* synchrotron powder diffraction patterns of LiV_3O_8 as positive electrode in an electrochemical Na-cell using a Na negative electrode during galvanostatic cycling at C/10 together with the corresponding voltage profile *vs*. the Na content in the material. A red ellipse shows the appearance of new Bragg reflections.

At low *x*, Rietveld analysis of LiV_3O_8 in all cells was based on the structural model of pristine LiV_3O_8. Additional reflections that appear upon further intercalation (including the aforementioned signal at $d \approx 7$ Å) are ascribed to the closely related $Na_{0.7}Li_{0.7}V_3O_8$ structure [21], hence leading to the two-phase structural model containing initial LiV_3O_8 and $Na_{0.7}Li_{0.7}V_3O_8$. In the Na-cell, the second phase appears in $Na_xLiV_3O_8$ at the total amount of Na of about $x \approx 0.25$, i.e., at 2.4 V *vs*. Na^+/Na. At this voltage, the minimum of $\tilde{D}_{Na}$ was also observed (Fig. 3a). The most significant difference between the crystal structures of $Na_{0.7}Li_{0.7}V_3O_8$ and LiV_3O_8 is reflected in the lattice parameter *a*, the distance between the neighboring vanadium oxygen layers, which is larger in the Na-containing structure.

The cell was measured two times during discharge and one time during charge (Fig. 5b). Interestingly, the amount of the second phase with the $Na_{0.7}Li_{0.7}V_3O_8$ structure increases upon cycling, reaching about 45% at the end of the first discharge and remains nearly unchanged during further cycling. The evolution of the lattice parameters upon cell discharge and charge was well reproducible. After the first charge, the cell parameters of the LiV_3O_8 phase are nearly the same as in the pristine material. Therefore, cell expansion and shrinkage occurs because of the insertion and subsequent removal of Na^+ cations. The initial Li^+ cations seem to be much stronger bonded in the structure.

Both LiV_3O_8-like and $Na_{0.7}Li_{0.7}V_3O_8$-like phases show changes in cell parameters upon further Na-insertion. While the former phase shows dissimilar behavior (its *a* parameter decreases, whereas the *b* and *c* parameters increase), the latter phase demonstrates cell expansion along all three directions. The cell volumes of both phases evolve in a similar manner, indicating that nearly the same amount of Na^+ ions is intercalated. It was not possible to remove the inserted Na completely during

cell charge, about 20% of Na according to the GCPL-measurements always remained in the material. This observation may indicate a higher thermodynamic stability of the partially sodiated $Na_{x\approx0.2}LiV_3O_8$ phase in comparison to the pure LiV_3O_8.

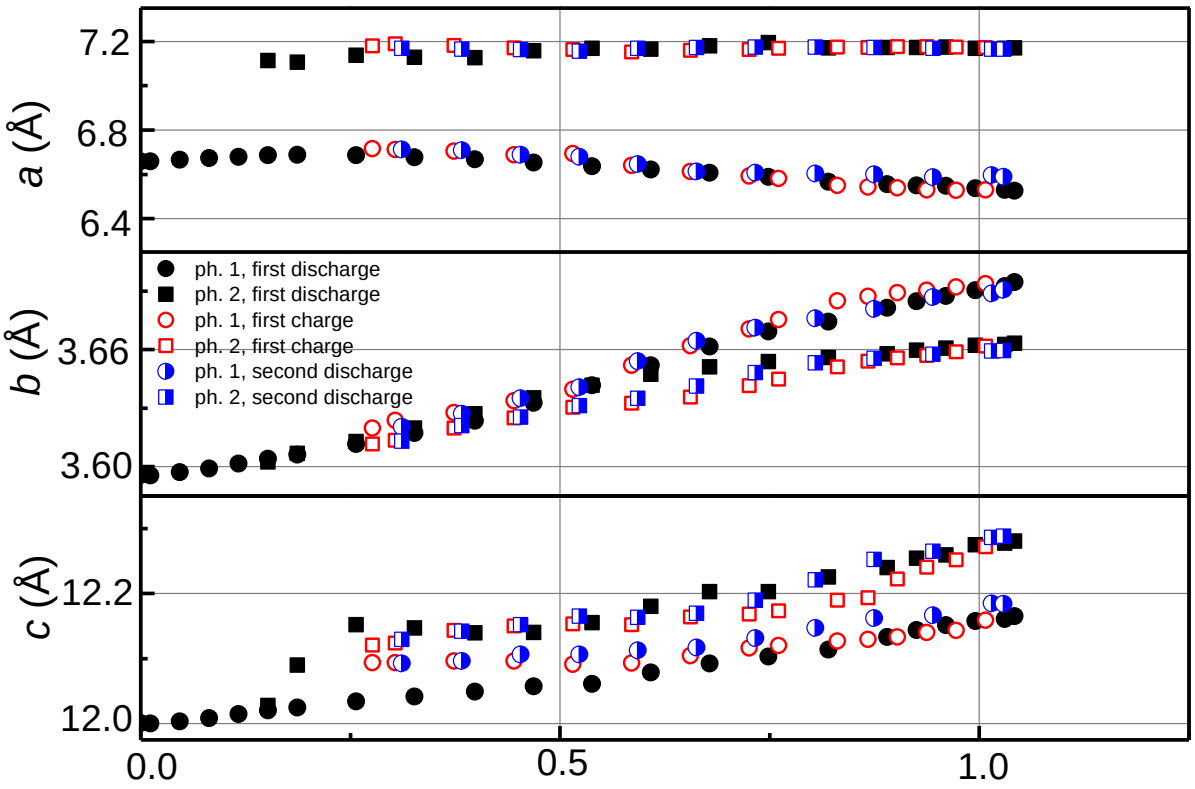

Figure 5b. Evolution of the lattice parameters of $Na_xLiV_3O_8$ depending on the total Na-content during electrochemical Na insertion and removal. Phase I corresponds to the initial LiV_3O_8, phase II appears after 0.2Na/f.u. is inserted into the material. The Na amount in the sample was calculated from the current flow in the galvanostatic experiment.

3. Electrochemical characterization of LiV_3O_8 in hybrid Li, Na-ion cells

In order to compare room-temperature kinetics of Li^+ and Na^+ intercalation into LiV_3O_8, we measured the Li^+ diffusion coefficient in LiV_3O_8 in a Li-cell, and a total diffusion coefficient $\tilde{D}_{tot.}$ in a hybrid cell with 50%Li50%Na electrolyte composition using GITT. The results are plotted together with $\tilde{D}_{Na}$ in Fig. 6. The voltage values for the Li-cell were shifted by -0.3 V to adjust the voltage reference to Na^+/Na.

In all cases, changes in chemical diffusion coefficients with voltage are extremely nonlinear. The Li-cell shows several minima; two small ones around 2.45-2.50 V and two deep ones between 2.3 and 2.05 V. Our $\tilde{D}_{Li}$ values are in good agreement with

literature data for lithiated $Li_{1+x}V_3O_8$, lying between $\tilde{D}_{Li}$ ~ 10^{-8} cm^2s^{-1} for $Li_{1.2}V_3O_8$ [17] and $\tilde{D}_{Li}$ ~ 10^{-13} cm^2s^{-1} for $Li_{3.6}V_3O_8$ [34]. Since $\tilde{D}_{Na}$ is of the same magnitude or even higher than $\tilde{D}_{Li}$, we can anticipate a co-intercalation of both Li^+ and Na^+ cations into LiV_3O_8 in a hybrid cell due to these very similar kinetics parameters, provided that both lithiated and sodiated phases have similar free energies. Actually, total chemical diffusion coefficients in the Li,Na-hybrid cell merge features from both $\tilde{D}_{Li}$ and $\tilde{D}_{Na}$ (Fig. 6) showing a minimum at 2.5 V like $\tilde{D}_{Li}$ but no minimum below 2.4 V that is similar to $\tilde{D}_{Na}$. Therefore, at least below 2.4 V a co-intercalation of Na^+ into LiV_3O_8 may be expected.

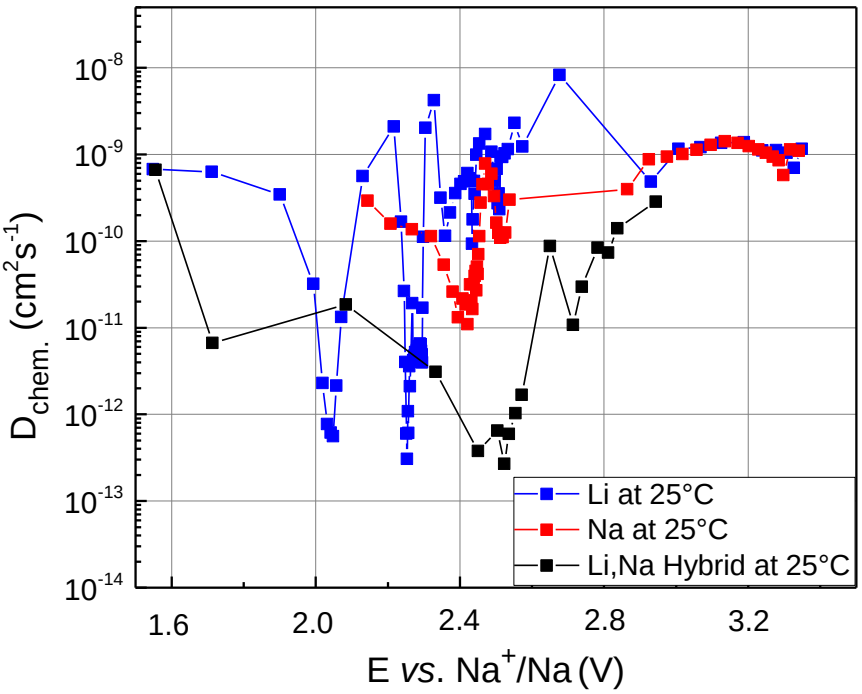

Figure 6. Comparison of Na^+, Li^+ and total diffusion coefficients in LiV_3O_8 at 25 °C in pure Na-, Li- and a hybrid Li,Na-cell with 50%Li50%Na electrolyte composition plotted *vs*. Na^+/Na (with a shift of -0.3 V for the Li-cell to adjust the voltage reference to Na^+/Na).

Four electrolyte compositions with different Li to Na contents (100%Li, 80%Li20%Na, 50%Li50%Na, 20%Li80%Na) were tested in electrochemical cells with a Na negative electrode. The first cation insertion/extraction in/from $A_xLiV_3O_8$ (*A* = Li and Na) together with the reference charge-discharge curve of a Li-cell with the $LiClO_4$ electrolyte and Li-anode are presented in Fig. 7a. The *x*-value is calculated from the charge that passes through the working electrode during cell discharge and charge.

Therefore, it depends only on the charge of the inserted cations and does not discriminate between the Li^+ or Na^+ ions entering the structure. The lower cut-off voltage of 1.6 V *vs*. Na^+/Na was chosen in order to avoid materials amorphisation.

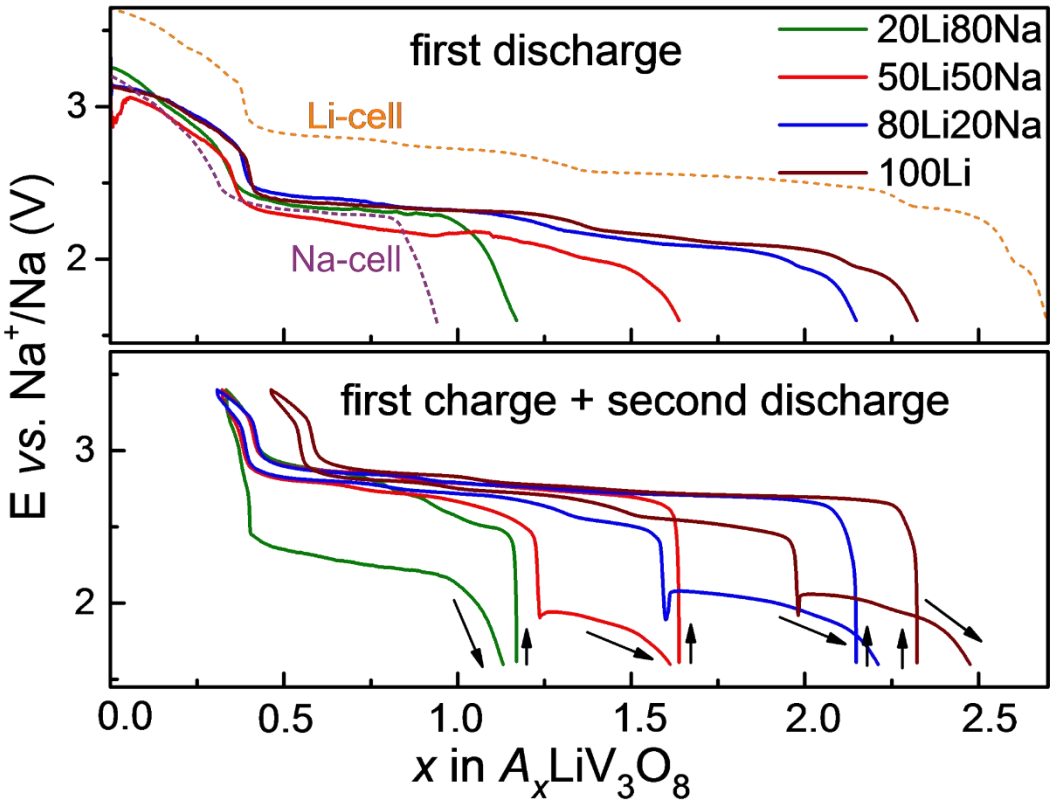

Figure 7a. First discharge-charge cycles (C/10) of four hybrid cells with a Na negative electrode and different Li to Na ratios in the electrolyte containing $LiClO_4$ and $NaClO_4$ salts with the total amount of 1M in PC. Since both Li and Na can be accommodated by the LiV_3O_8 structure, the total formula of the intercalated phase was denoted as $ALiV_3O_8$, where *A* stands for both Li and Na. Voltage profiles of a pure Li-cell and a pure Na-cell were added for comparison (dashed orange and purple lines, respectively).

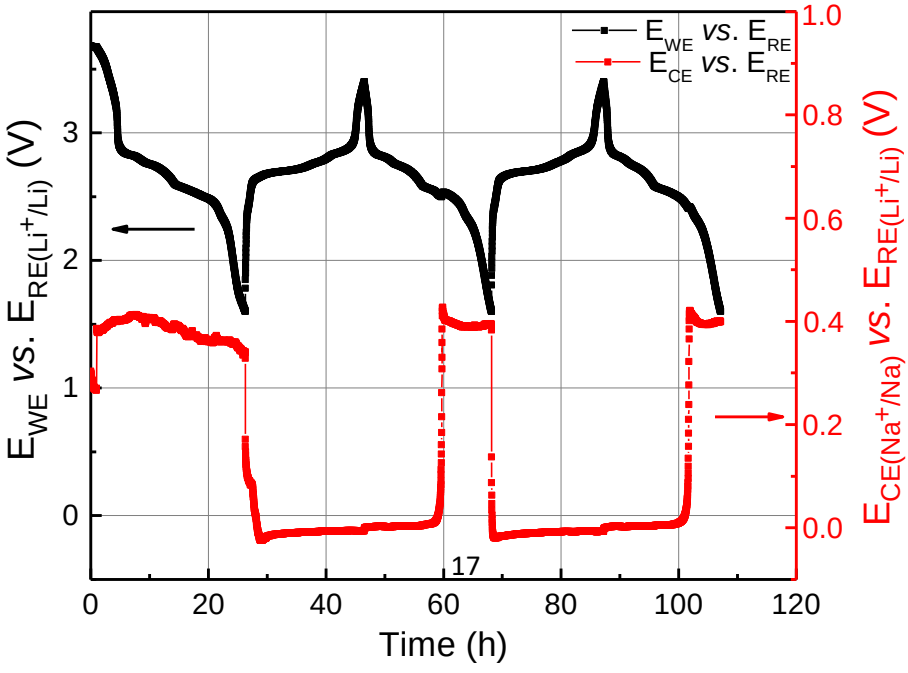

Figure 7b. Discharge-charge profile as a function of time for a three-electrode hybrid cell with LiV_3O_8 as a working electrode (WE), Na anode as a counter electrode (CE), Li plate as a reference electrode (RE), and 50%Li50%Na electrolyte composition. The black curve shows the potential between LiV_3O_8 and RE, the red curve - the potential between CE and RE.

The entire amount *x* of the cations intercalated into the $A_xLiV_3O_8$ electrode in hybrid cells against a Na negative electrode during the first discharge depends strongly on the Li content in the electrolyte. It ranges from x = 1.0 for cells with the pure Na-based electrolyte to x = 2.35 for cells with pure Li-based electrolyte. Interestingly, the width of the range preceding the voltage plateau (x<0.4) is independent of both anode (Li or Na) and electrolyte composition.

The whole discharge capacity of a Li-cell with a Li-based negative electrode and $LiClO_4$ electrolyte is somewhat higher than the capacity of a hybrid cell against a Na-electrode and $LiClO_4$ electrolyte (Fig. 7a top). The first cell charge occurs at nearly the same cell voltage of 2.75 V for cells with different Li and Na amounts in the electrolyte, except for the cell with 20%Li80%Na electrolyte composition, where two plateaus at 2.50 and 2.75 V are observed, as represented in Fig. 7a bottom. However, the electrolyte composition significantly affects the second cell discharge. The cells with at least 50% $LiClO_4$ in the electrolyte demonstrate a two-step process with the first broad discharge plateau at 2.8 V and a narrower second one at about 2.0 V. In contrast, cation insertion into the cell with only 20% $LiClO_4$ in the electrolyte occurs as a one-step process at 2.4 V. Two scenarios are possible: *i*) the formation of a new $(Li,Na)_xLiV_3O_8$ phase with the Li,Na cation ordering when sufficient amount of Li is present in the electrolyte; *ii*) anodic deposition of Li during the first cell charge, and the subsequent cycling of the positive electrode against metallic Li. In order to prove this statement, a three-electrode cell with LiV_3O_8 as a working electrode (WE), metallic Na as a counter electrode (CE), metallic Li as a reference electrode (RE), and an electrolyte containing 50% $LiClO_4$ and 50% $NaClO_4$ was cycled with the C/10 rate. Fig. 7b depicts time evolution of the potential between LiV_3O_8 and RE, and between CE and RE.

At the beginning of the first cell discharge, the discrepancy between $E_{CE(Na+/Na)}$ and $E_{RE(Li+/Li)}$ of about 0.4 V corresponds to the expected difference between the Li^+/Li and the Na^+/Na redox couples. However, upon first cell charge the discrepancy between $E_{CE(Na+/Na)}$ and $E_{RE(Li+/Li)}$ nearly vanishes and remains small during the whole charge process and during the most part of the next discharge process as well. Only below about 2.1 V *vs*. Na^+/Na (Fig. 7a bottom) or about 2.5 V *vs*. Li^+/Li reference electrode (Fig. 7b), the difference between $E_{CE(Na+/Na)}$ and $E_{RE(Li+/Li)}$ again reaches the initial value of 0.4 V. Therefore, the first cell discharge in the Li,Na-hybrid cells occurs against the Na^+/Na redox pair, regardless of the electrolyte composition. The first charge cycle is accompanied by Li-plating on the Na-anode, provided that the Li-content in the electrolyte exceeds 20%. This behavior results in the increase in cell voltage and, therefore, in the enrichment of the electrolyte with Na-cations. The subsequent cation intercalation into LiV_3O_8 occurs against the Li^+/Li pair until lithium is completely dissolved in the electrolyte. Then the Na^+/Na redox pair determines the cell voltage again. At the beginning of the second cell discharge, the electrolyte still contains an excess of Na-cations, which are likely intercalated first before the intercalation of Li starts. Li-plating was not observed in the cells with electrolytes containing 20% of $LiClO_4$ or less.

4. Structural evolution of LiV_3O_8 in hybrid Li,Na-cells upon cell discharge and charge

In situ synchrotron powder diffraction revealed structural changes already at the beginning of the cation intercalation. LiV_3O_8 electrodes were cycled in electrochemical hybrid Li,Na-cells against a Na counter electrode and, for comparison, in a Li-cell against Li-metal. For all hybrid cells, we focused on structural changes in LiV_3O_8 upon intercalation of nearly one cation (Li^+, Na^+ or both) per formula unit, since a pure Na-cell allows insertion of only one Na atom per formula unit. The cells were thus discharged down to 1.6 V *vs*. Na^+/Na (2.4 V *vs*. Li^+/Li for the Li-cell) and subsequently charged to 3.4 V, whereas for the pure Li cell the lower limit was set to 2.4 V where one atom per formula unit is intercalated. The ratios of $LiClO_4$

and $NaClO_4$ in the electrolyte of the hybrid cells were 80% to 20%, 50% to 50%, and 20% to 80%, respectively. As an example, the evolution of the diffraction patterns as a function of cell voltage for the hybrid Li,Na-cell with a Li-rich electrolyte (80%Li20%Na) is presented in Fig. 8a. The diffraction patterns of other cells, a typical structure refinement, and refined lattice parameters of the material in hybrid cells are shown in Fig. S8-S10.

The diffraction patterns suggest that each cell falls into one of the two groups depending on the electrolyte composition. In Li,Na-hybrid cells with a Na content ≥50% in the electrolyte, similar features as already discussed for pure Na-cells in section 2 (Fig. 5a) were observed. These include the appearance of lasting reflections at high *d*-values and reversible changes in the *d*-spacing of other reflections, indicating changes in cell volume. In the other cells, including the purely Li-cell and the Li,Na-hybrid cells with the Li-rich electrolyte, additional reflections appear only for a short time at the end of the intercalation process and disappear again during subsequent cation removal, see for example the reflection at $d \approx 3.30$ Å in Fig. 8a.

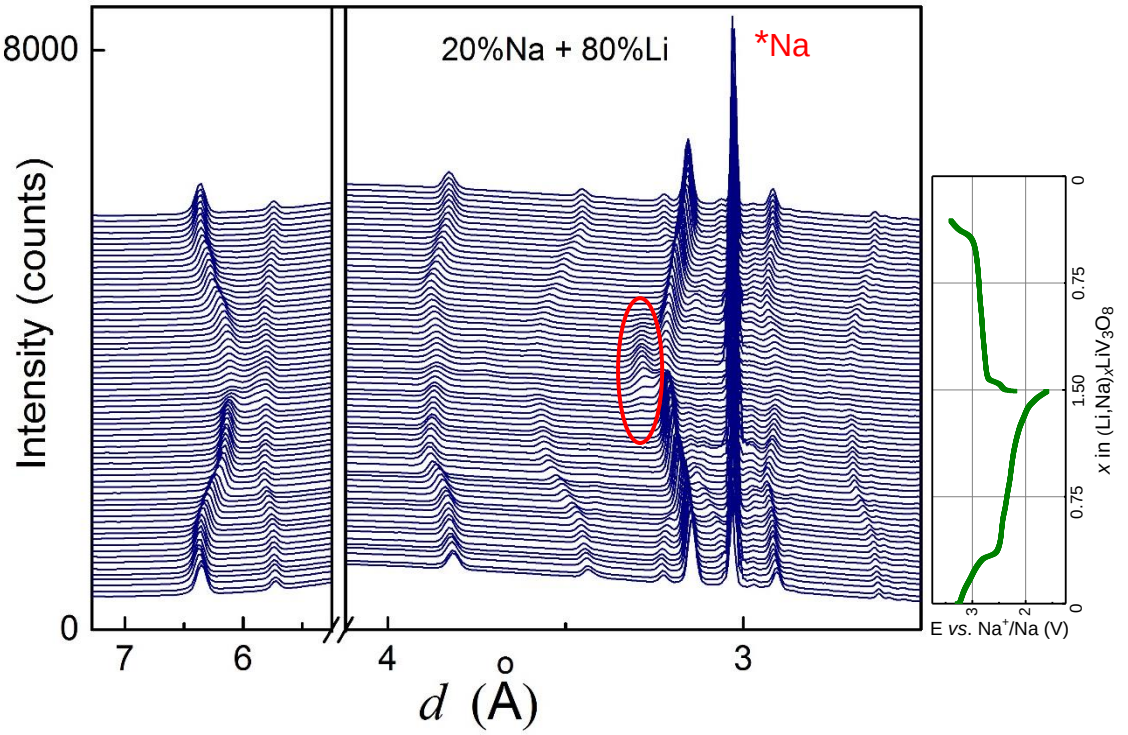

Figure 8a. *In situ* synchrotron powder diffraction patterns of LiV_3O_8 as positive electrode in the electrochemical hybrid Li,Na-cell with a 20%Na80%Li electrolyte composition and Na negative electrode during galvanostatic cycling at C/10 together with the voltage profile of the cell *vs*. (Li,Na) content in the material. A red ellipse shows the appearance of new Bragg reflections upon cation insertion.

Figure 8b shows the change of the lattice parameter *a* of LiV_3O_8 cycled in hybrid Li,Na-cells and in the Li-cell upon cell discharge and charge. In the case of the Li-cell and the hybrid cell with the 80%Li20%Na electrolyte composition, the Rietveld analysis was based on the structural model of the LiV_3O_8 phase almost up to the end of the discharge process. The second phase appears only at the end of the cell discharge that corresponds to $x \approx 1.25\text{-}1.3$ in $(Li,Na)_xLiV_3O_8$. Structure refinement in the two-phase region utilized the model containing the initial LiV_3O_8 and fully lithiated $Li_4V_3O_8$ phases, in agreement with earlier studies of the Li insertion process into LiV_3O_8 [35, 36]. This $Li_4V_3O_8$ phase completely disappeared upon the subsequent Li-removal. Since the evolution of the cell parameters for both cells, the purely Li- one and the hybrid one with the 80%Li20%Na electrolyte composition, occurs in a similar manner during the first discharge and charge, the insertion of Li^+ ions is proposed, whereas Na^+-ions remain inactive, even if they are present in the electrolyte.

The increase in the Na-content in the electrolyte to 50% changes the intercalation scenario towards the one observed in pure Na-cells. The second phase with a $Na_{0.7}Li_{0.7}V_3O_8$-like structure starts to form at *x*(Li, Na) ≈ 0.7 and 2.3 V, which is lower than the voltage where minimum value of the total chemical diffusion coefficient is observed.

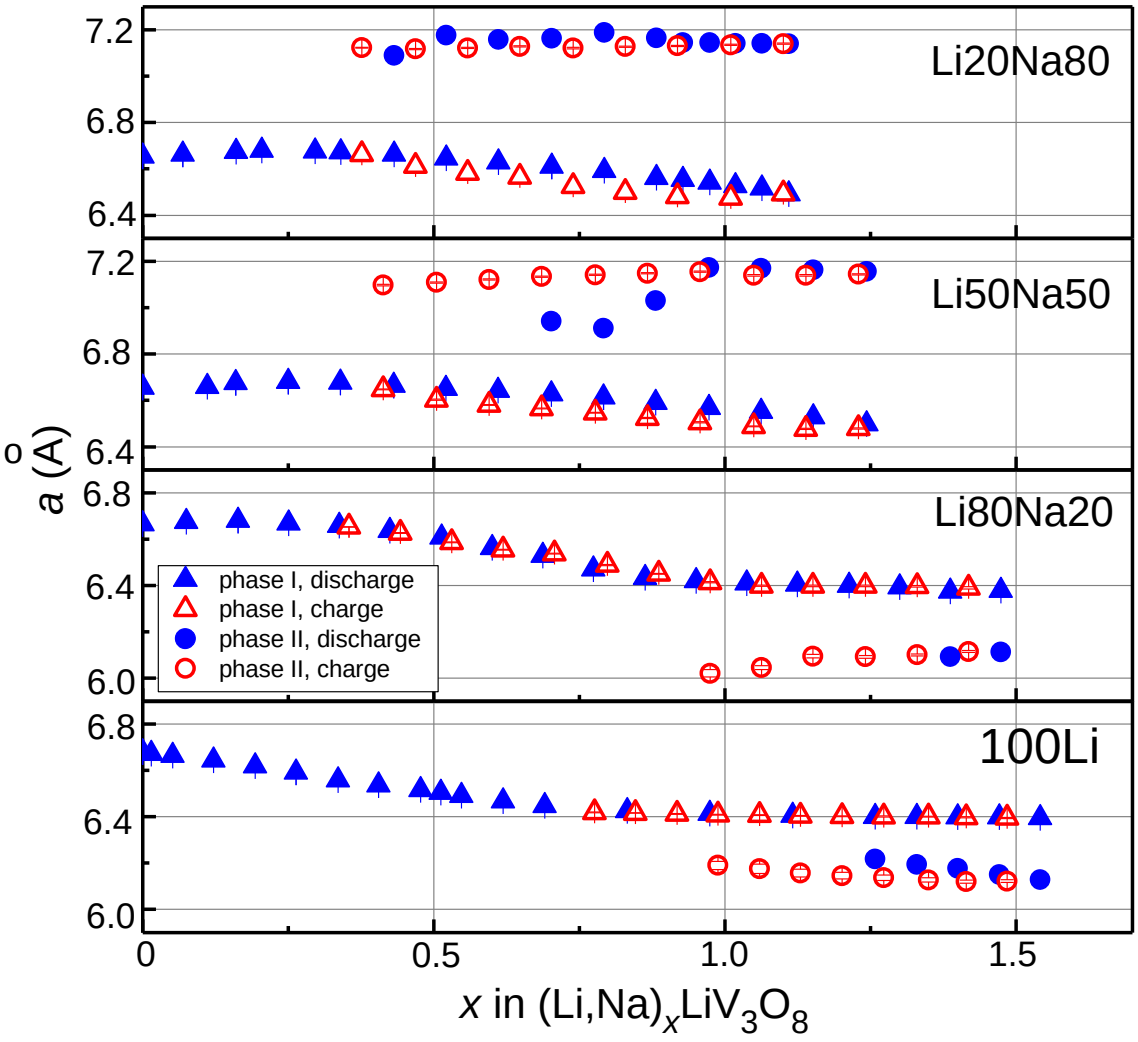

Figure 8b. Composition dependence of the lattice parameter *a* of LiV_3O_8 measured *in situ* during discharge and charge in a Li-cell with Li-anode and only Li-containing electrolyte (symbol Li), and in Li,Na-hybrid cells with Na-anode and different Li and Na contents in the electrolyte.

5. Stability of LiV_3O_8 and $Na_{0.7}Li_{0.7}V_3O_8$ structure types towards cation intercalation

The formation of the $Na_{0.7}Li_{0.7}V_3O_8$-like phase upon intercalation from Na-rich electrolytes implies that the Na-containing structure may be more suitable for the Na intercalation. We verified this conjecture by an *ab initio* evaluation of total energies for several ordered structural models. Both LiV_3O_8-like and $Na_{0.7}Li_{0.7}V_3O_8$-like phases were tested against the intercalation of one Li or one Na ion per formula unit starting from the fully oxidized V^{+5}-containing composition. Detailed structural data and crystallographic projections of the models can be found in the Supporting Information, section 4.

In the case of LiV_3O_8, the intercalated cations were placed into the (1/2, 1/4, 0) position, i.e., in the interlayer space between the two inherent Li^+ ions. Other starting positions were tried as well, but all of them converged to the same structure, where 2 Li^+ ions (or one Li^+ and one Na^+ ion) per formula unit are distributed between the $[V_3O_8]$ layers. The intercalation of Li^+ cations has minor effect on the structure, in agreement with Ref. [37]. In opposite to this, Na intercalation triggers distortions of the $[V_3O_8]$ layers to achieve longer Na–O distances, which are required for the larger Na^+ ions. The *a* and *c* lattice parameters increase by 0.20–0.25 Å, whereas the *b* parameter changes insignificantly.

In the case of $Na_{0.7}Li_{0.7}V_3O_8$, we considered the structure from Ref. [21] as the intercalated one. This structure features strong cation disorder, which cannot be treated *ab initio*. Therefore, Na and Li were placed into two positions having largest occupancies in the experimental structure, and these positions were treated as fully occupied resulting in the idealized $NaLiV_3O_8$ composition. The removal of Na again triggered a major re-arrangement of the $[V_3O_8]$ layers, and the unit cell along the interlayer direction *a* shrinked by 0.35 Å. In contrast, the removal of Li changed the lattice parameters by less than 0.1 Å.

The LiV_3O_8 structure is prone to Li intercalation. We calculated the redox potential of 3.04 V *vs*. Li^+/Li compared to 2.39 V *vs*. Na^+/Na for the Na intercalation. The $Na_{0.7}Li_{0.7}V_3O_8$ structure shows an opposite trend, 3.06 V *vs*. Li^+/Li and 3.76 V *vs*. Na^+/Na for the Li and Na intercalation, respectively. Total energy of $NaLiV_3O_8$ with the LiV_3O_8-type structure is 0.55 eV/f.u. higher than that with the $Na_{0.7}Li_{0.7}V_3O_8$-type structure. This huge difference should be traced back to the different buckling of the $[V_3O_8]$ layers. The $Na_{0.7}Li_{0.7}V_3O_8$-type structure is capable of accommodating larger Na^+ ions in an octahedrally coordinated position with Na–O distances of 2.2–2.4 Å. On the other hand, the Na-intercalated LiV_3O_8-type structure reveals three Na–O distances below 2.2 Å that are energetically unfavorable.

We conclude that the LiV_3O_8-type phase is prone to the intercalation of Li, whereas the $Na_{0.7}Li_{0.7}V_3O_8$-type phase is prone to the intercalation of Na. Together they may support an efficient operation of hybrid cells with the simultaneous intercalation of both ions.

Discussion

Successful operation of a hybrid-ion battery requires that two ions are present in the electrolyte and exhibit different behavior with respect to their redox potentials and diffusion in electrode materials. In the present work, the comparison of Li- and Na-ion batteries assembled with a LiV_3O_8 positive electrode displayed very similar chemical diffusion coefficients for Li and Na at room temperature as well as similar activation energies for the cation transport in the material. Therefore, co-intercalation of Na^+ and Li^+ cations in a Li,Na-hybrid cell can be expected with similar availability of both cations, at least due to kinetic reasons. Actually, *in situ* synchrotron diffraction measurements on the hybrid cell with a 50%Li50%Na electrolyte revealed minor Li-insertion at the beginning of the discharge followed by a predominant Na-insertion, which is reflected in the formation of a second phase of the $Na_{0.7}Li_{0.7}V_3O_8$ type. In contrast, upon discharge of the cell with a Li-enriched electrolyte, only Li insertion occurs, providing capacity values comparable with a pure Li-cell.

Co-intercalation of different cations in hybrid cells has been reported in the literature previously. For example, co-intercalation of Li^+ and Mg^{2+} ions was observed in hybrid Li,Mg-cells with a Mg-anode, Li- and Mg-containing dual electrolyte, and a nanosized $Li_4Ti_5O_{12}$ positive electrode [11], since the Mg-insertion is energetically favorable [38], but the Mg^{2+}-diffusion is several orders of magnitude slower than the Li^+-diffusion [39]. A macrosized $Li_4Ti_5O_{12}$ positive electrode suppressed the Mg-insertion and led to the intercalation of Li as the dominant reaction [11]. In the case of LiV_3O_8, the co-intercalation of Li and Na cannot be eliminated by increasing the particle size, because of comparable diffusion rates of Li^+ and Na^+ ions in the bulk, and close energies of the intercalated structures.

In our hybrid cells with a Li-content of 50% and higher, Li-deposition during cell charge was observed, accompanied by a cell voltage jump of about 0.33 V, which corresponds to the difference between the standard electrode potentials of the Li^+/Li and Na^+/Na redox couples. During subsequent cell discharge, Li starts to dissolve, and after its complete dissolution the cell potential decreases abruptly back to the value corresponding to the Na^+/Na pair. The observed effect contradicts thermodynamic considerations, which clearly predict Na-deposition first. Remarkably, the same small difference in redox potentials of 0.33 V between the Na^+/Na and Mg^{2+}/Mg redox couples did not induce co-deposition of Na on the Mg-anode in a hybrid Na,Mg-ion cell [40]. On the other hand, in electrochemical cells containing Al^{3+} and Li^+ cations in the electrolyte, electrodeposition of either Al or Li was observed

depending on electrolyte solvents, despite the larger difference in standard electrode potentials of Li^+/Li and Al^{3+}/Al couples of 1.38 V [41]. Therefore, in such dual electrochemical cells kinetics definitely outweighs thermodynamic parameters.

Already in the late 1970s the crucial role of a solid-electrolyte-interface (SEI) for the corrosion rate of the metal, the mechanism of plating-stripping process, and even for the half-cell potential was identified [41]. The composition of the SEI film is mostly influenced by the electrolyte composition. Recently, it was shown that symmetrical Li/Li cells with conventional carbonate-containing electrolytes exhibit low polarization and smooth charge-discharge curves at low and high current densities, while large overpotentials were observed for Na/Na cells even at low current densities, which was attributed to different stabilities of the individual SEIs on Li and Na [42].

Fortunately, the efficiency of Na-anodes can also be significantly improved by a combination of appropriate electrolyte salts and electrolyte solvents, as newly demonstrated for Na cells with $NaPF_6$ in glymes (mono-, di-, and tetraglyme), yielding a stable inorganic SEI film composed of Na_2O and NaF [43]. Therefore, an appropriate electrolyte composition of Li and Na salts can be found for hybrid Li,Na-cells, in order to avoid co-deposition of Li and Na metals on the Na anode.

To summarize, two main issues can be concluded from studies of Li,Na-hybrid cells with a LiV_3O_8 positive electrode. First, co-intercalation of Li- and Na-ions into microsized LiV_3O_8 must be expected due to thermodynamic and kinetic reasons with similar availability of both cations. Since only about 1 Na per LiV_3O_8 can be reversibly intercalated in contrast to about 3 Li without material amorphization, a Li-enriched electrolyte must be employed. Second, a Li-plating on the Na-anode may be reduced by choosing proper electrolytes.

Conclusions

Lithium trivanadium (V) oxide, LiV_3O_8, prepared *via* a conventional solid-state route, was tested for the first time as positive electrode in Na- and hybrid Li,Na-ion batteries. In a pure Na-cell, it revealed a reversible electrochemical insertion of about 1 Na per formula unit without any deterioration of the material, thus yielding a reversible capacity of 60 mAh/g. Further Na intercalation leads to a gradual amorphisation with each cycle, reflected in XRD and XPS studies, and in a less stable cycling behavior, which is similar to that of ball-milled amorphous LiV_3O_8. Both Li^+ and Na^+ ions show similar transport properties in LiV_3O_8 regarding the chemical

diffusion coefficients and activation energies. Therefore, co-intercalation of Li^+ and Na^+ ions into LiV_3O_8 is expected in hybrid Li,Na-ion batteries.

In situ synchrotron diffraction on Na- and hybrid Li,Na-cells with Na metal as negative electrode and a dual Li,Na-containing electrolyte showed the formation of a second phase upon the first cell discharge. This phase resembles lithiated $Li_4V_3O_8$ in Li-rich electrolytes and a mixed $Li_{0.7}Na_{0.7}V_3O_8$ phase in Na-rich electrolytes. Interestingly, the "$Li_4V_3O_8$"-type phase completely disappeared during cell charge, while the $Li_{0.7}Na_{0.7}V_3O_8$-type phase remained in the material upon further cycling. Hybrid Li,Na-cells with a Li-content in the electrolyte of 50% and higher demonstrated Li-deposition on the Na-anode during cell charge. Upon cell discharge, Li is completely dissolved in the electrolyte.

Acknowledgment

This work has benefited from financial support within the BMBF project "DESIREE", grant number 03SF0477B. The authors are indebted to Dr. T. Jaumann (IFW Dresden, Germany) for help in performing the SEM studies, and A. Voss (IFW Dresden, Germany) for performing the ICP-OES analyses. AT was supported by Federal Ministry of Education and Research through the Sofja Kovalevskaya award of the Alexander von Humboldt Foundation.

References

[1] M. D. Slater, D. Kim, E. Lee, C. S. Johnson, *Adv. Function. Mater*. 2013, 23, 947-958 Sodium-Ion Batteries.

[2] S.-W. Kim, D.-H. Seo, H. Ma, G. Ceder, Electrode Materials for Rechargeable Sodium-Ion Batteries: Potential Alternatives to Current Lithium-Ion Batteries, *Adv. Energy Mater.* 2 (2012) 710-721.

[3] V. Palomares, P. Serras, I. Villaluenga, K. B. Hueso, J. Carretero-Gonzalez, T. Rojo, Na-ion batteries, recent advances and present challenges to become low cost energy storage systems, *Energy Environ. Sci.* 5 (2012) 5884-5901.

[4] R. D. Shannon, Revised effective ionic radii and systematic studies of interatomic distances in halides and chalcogenides, *Acta Cryst.* A 32 (1976) 751-762.

[5] F. Sagane, T. Abe, Y. Iriyama, Z. Ogumi, Li^+ and Na^+ transfer through interfaces between inorganic solid electrolytes and polymer or liquid electrolytes, *J. Power Sources* 146 (2005) 749–752.

[6] H. P. Latscha, H. A. Klein, M. Mutz, Allgemeine Chemie : Chemie-Basiswissen I. Springer-Verlag, Berlin, 2011.

[7] Y. Zhu, Y. Xu, Y. Liu, C. Luo, C. Wang, Comparison of electrochemical performances of olivine $NaFePO_4$ in sodium-ion batteries and olivine $LiFePO_4$ in lithium-ion batteries, *Nanoscale* 5 (2013) 780-787.

[8] Y. Cheng, Y. Shao, J.-G. Zhang, V. L. Sprenkle, J. Liu, G. Li, High performance batteries based on hybrid magnesium and lithium chemistry, *Chem. Commun.* 50 (2014) 9644-9646.

[9] S. Su, Z. Huang, Y. NuLi, F. Tuerxun, J. Yang, J. Wang, A novel rechargeable battery with a magnesium anode, a titanium dioxide cathode, and a magnesium borohydride/tetraglyme electrolyte, *Chem. Commun.* 51 (2015) 2641-2644.

[10] Y. Cheng, D. Choi, K. S. Han, K. T. Mueller, J. Zhang, V. L. Sprenkle, J. Liu, G. Li, Toward the Design of High Voltage Magnesium-Lithium Hybrid Batteries using Dual-Salt Electrolytes, *Chem. Commun.* 52 (2016) 5379-5382.

[11] H.-R. Yao, Y. You, Y.-X. Yin, L.-J. Wan, Y.-G. Guo, Rechargeable dual-metal-ion batteries for advanced energy storage, *Phys.Chem.Chem.Phys.* 18 (2016) 9326-9333.

[12] M. Walter, K. V. Kravchyk, M. Ibáñez, M. V. Kovalenko, Efficient and Inexpensive Sodium-Magnesium Hybrid Battery, *Chem. Mater.* 27 (2015) 7452-7458.

[13] H. Dong, Y. Li, Y. Liang, G. Li, C.-J. Sun, Y. Ren, Y. Lu, Y. Yao, A magnesium–sodium hybrid battery with high operating voltage, *Chem. Commun.* 52 (2016) 8263-8266.

[14] L. Chen, Q. Gu, X. Zhou, S. Lee, Y. Xia, Z. Liu, New-concept batteries based on aqueous Li^+/Na^+ mixed-ion electrolytes, *Sci. Rep.* 3 (2013) 1946-1948.

[15] Y. Yao, P. Yang, X. Bie, C. Wang, Y. Wei, G. Chen, F. Du, High capacity and rate capability of a layered Li_2RuO_3 cathode utilized in hybrid Na^+/Li^+ batteries, *J. Mater. Chem. A* 3 (2015) 18273-18278.

[16] G. Pistoia, S. Panero, M. Tocci, R.V. Moshtev, V. Manev, Solid Solutions $Li_{1+x}V_3O_8$ as cathodes for high rate secondary Li Batteries, *Solid State Ion.* 13 (1984) 311–318.

[17] J. Kawakita, T. Miura, T. Kishi, Lithium insertion and extraction kinetics of $Li_{1+x}V_3O_8$, *J. Power Sources* 83 (1999) 79-83.

[18] G. Yang, G. Wang, W. H. Hou, Microwave solid-state synthesis of LiV_3O_8 as cathode material for lithium batteries, *J. Phys. Chem. B* 109 (2005) 11186-11196.

[19] J. Köhler, H. Makihara, H. Uegaito, H. Inoue, M. Toki, LiV_3O_8: characterization as anode material for an aqueous rechargeable Li-ion battery system, *Electrochim. Acta* 46 (2000) 59-65.

[20] L. A. de Picciotto, K.T. Adendorff, M. M. Thackeray, und D. C. Liles, Structural characterization of $Li_{1+x}V_3O_8$ insertion electrodes by single-crystal X-ray diffraction, *Solid State Ion.* 62 (1993) 297–307.

[21] M. Schindler, F. C. Hawthorne, M. A. Alexander, R. A. Kutluoglu, P. Mandaliev, N. M. Halden, R. H. Mitchell, Na-Li-[V_3O_8] insertion electrodes: structure and diffusion pathways, *J. Solid State Chem*. 179 (2006) 2616–2628.

[22] W. Weppner, R. A. Huggins, Determination of the kinetic parameters of mixed-conducting electrodes and application to the system Li_3Sb, *J. Electrochem. Soc.* 124 (1977) 1569-1578.

[23] X. M. Jian, H. Q. Wenren, S. Huang, S. J. Shi, X. L. Wang, C. D. Gu, J. P. Tu, Oxalic acid-assisted combustion synthesized $LiVO_3$ cathode material for lithium ion batteries, *J. Power Sources* 246 (2014) 417-422.

[24] F. Fauth, I. Peral, C. Popescu, M. Knapp, The new Material Science Powder Diffraction beamline at ALBA Synchrotron, *Powder Diffr.* 28 (2013) S360–S370.

[25] M. Herklotz, J. Weiss, E. Ahrens, M. Yavuz, L. Mereacre, N. Kiziltas-Yavuz, C. Draeger, H. Ehrenberg, J. Eckert, F. Fauth, L. Giebeler, M. Knapp, A novel high-throughput setup for *in situ* powder diffraction on coin cell batteries, *J. Appl. Cryst.* 49 (2016) 340-345.

[26] T. Roisnel, J. Rodriguez-Carvajal, WinPLOTR: a Windows tool for powder diffraction pattern analysis, *Mater. Sci. Forum* 378-381 (2001) 118-123.

[27] G. Kresse, J. Furthmüller, Efficiency of ab-initio total energy calculations for metals and semiconductors using a plane-wave basis set, *Comput. Mater. Sci*. 6 (1996) 15.

[28] G. Kresse, J. Furthmüller, Efficient iterative schemes for *ab initio* total-energy calculations using a plane-wave basis set, *Phys. Rev. B* 54 (1996) 11169.

[29] J. P. Perdew, K. Burke, M. Ernzerhof, Generalized Gradient Approximation Made Simple, *Phys. Rev. Lett*. 77 (1996) 3865.

[30] P. Vanysek, *Electrochemical series*, in: *CRC Handbook of Chemistry and Physics* (D. R. Lide, Ed.), 87 ed., CRC Press, Boca Raton (1998).

[31] J.-C. Dupin, D. Gonbeau, P. Vinatier, A. Levasseur, Systematic XPS studies of metal oxides, hydroxides and peroxides, *Phys. Chem. Chem. Phys.* 2 (2000) 1319−1324.

[32] S. Oswald, Binding energy referencing for XPS in alkali metal-based battery materials research (I): Basic model investigations, *Appl. Surf. Sci*. 351 (2015) 492–503.

[33] S. Oswald, D. Mikhailova, F. Scheiba, P. Reichel, A. Fiedler, H. Ehrenberg, XPS investigations of electrolyte/electrode interactions for various Li-ion battery materials, *Anal. Bioanal. Chem.* 400 (2011) 691–696.

[34] A. Pan, J. Liu, J.-G. Zhang, G. Cao, W. Xu, Z. Nie, X. Jie, D. Choi, B. W. Arey, C. Wange, S. Liang, Template free synthesis of LiV_3O_8 nanorods as a cathode material for high-rate secondary lithium batteries, *J. Mater. Chem*. 21 (2011) 1153-1161.

[35] J. Kawakita, Y. Katayama, T. Miura, T. Kishi, Structural properties of $Li_{1+x}V_3O_8$ upon lithium insertion at ambient and high temperature, *Solid State Ionics* 107 (1998) 107, 145–152.

[36] M. Shui, W. Zheng, J. Shu, Q. Wang, S. Gao, D. Xu, L. Chen, L. Feng, Y. Ren, Synthesis, spectral character, electrochemical performance and in situ structure studies of $Li_{1+x}V_3O_8$ cathode material prepared by tartaric acid assisted sol–gel process, *Mat. Res. Bull.* 47 (2012) 2455-2459.

[37] T. Jiang, M.L. Falk, Calculations of the thermodynamic and kinetic properties of $Li_{1+x}V_3O_8$, *Phys. Rev. B* 85 (2012) 245111.

[38] N. Wu, Y.-C. Lyu, R.-J. Xiao, X. Yu, Y.-X. Yin, X.-Q. Yang, H. Li, L. Gu, Y.-G. Guo, A highly reversible, low-strain Mg-ion insertion anode material for rechargeable Mg-ion batteries, *NPG Asia Mater*. 6 (2014) e120.

[39] N. Wu, Z.-Z. Yang, H.-R. Yao, Y.-X. Yin, L. Gu and Y.-G. Guo, Improving the Electrochemical Performance of the $Li_4Ti_5O_{12}$ Electrode in a Rechargeable Magnesium Battery by Lithium–Magnesium Co-Intercalation, *Angew. Chem*. *Int. Ed*. 54 (2015) 5757–5761.

[40] H. Dong, Y. Li, Y. Liang, G. Li, C.-J. Sun, Y. Ren,Y. Lu, Y. Yao, A magnesium–sodium hybrid battery with high operating voltage, *Chem. Commun.* 52 (2016) 8263-8266.

[41] E. Peled, The Electrochemical Behavior of Alkali and Alkaline Earth Metals Battery Systems - The Solid Electrolyte Interphase Model, *J. Electrochem. Soc*. 126 (1979) 2047-2051.

[42] D. I. Iermakova, R. Dugas, M. R. Palacín, A. Ponrouch, On the Comparative Stability of Li and Na Metal Anode Interfaces in Conventional Alkyl Carbonate Electrolytes, *J. Electrochem. Soc*.162 (2015) A7060-A7066.
[43] Z. W. Seh, J. Sun, Y. Sun, Y. Cui, A Highly Reversible Room-Temperature Sodium Metal Anode, *ACS Cent. Sci*. 1 (2015) 449−455.